

● Original Contribution

SPATIOTEMPORAL ASSESSMENT OF THE CELLULAR SAFETY OF CAVITATION-BASED THERAPIES BY PASSIVE ACOUSTIC MAPPING

CAMERON A.B. SMITH, and CONSTANTIN C. COUSSIOS

Institute of Biomedical Engineering, Department of Engineering Science, University of Oxford, Oxford, United Kingdom

(Received 30 August 2019; revised 9 December 2019; in final form 13 January 2020)

Abstract—Many useful therapeutic bio-effects can be generated using ultrasound-induced cavitation. However, cavitation is also capable of causing unwanted cellular and vascular damage, which should be monitored to ensure treatment safety. In this work, the unique opportunity provided by passive acoustic mapping (PAM) to quantify cavitation dose across an entire volume of interest during therapy is utilised to provide setup-independent measures of spatially localised cavitation dose. This spatiotemporally quantifiable cavitation dose is then related to the level of cellular damage generated. The cavitation-mediated destruction of equine red blood cells mixed with one of two types of cavitation nuclei at a variety of concentrations is investigated. The blood is placed within a 0.5-MHz ultrasound field and exposed to a range of peak rarefactional pressures up to 2 MPa, with 50 to 50,000 cycle pulses maintaining a 5% duty cycle. Two co-planar linear arrays at 90° to each other are used to generate 400- μ m-resolution frequency domain robust capon beamforming PAM maps, which are then used to generate estimates of cavitation dose. A relationship between this cavitation dose and the levels of haemolysis generated was found which was comparable regardless of the applied acoustic pressure, pulse length, cavitation agent type or concentration used. PAM was then used to monitor cellular damage in multiple locations within a tissue phantom simultaneously, with the damage–cavitation dose relationship being similar for the two experimental models tested. These results lay the groundwork for this method to be applied to other measures of safety, allowing for improved ultrasound monitoring of cavitation-based therapies. (E-mail: constantin.coussios@eng.ox.ac.uk) © 2020 The Author(s). Published by Elsevier Inc. on behalf of World Federation for Ultrasound in Medicine & Biology. This is an open access article under the CC BY license. (<http://creativecommons.org/licenses/by/4.0/>).

Key Words: Cavitation, Ultrasound, Acoustics, Passive acoustic mapping, Bio-effect, Safety, Microbubbles, Nano-scale cavitation nuclei, Haemolysis, Robust capon beamformer.

INTRODUCTION

Cavitation is capable of significantly enhancing drug delivery for brain, cardiovascular, oncological, transdermal and intracellular applications (Hynynen et al. 2001; Fan et al. 2012; Bazan-Peregrino et al. 2013; Sutton et al. 2013; Bhatnagar et al. 2016; Bian et al. 2017; Manaris et al. 2018; Stride and Coussios 2019), but can also generate potentially adverse bio-effects that need to be monitored to ensure treatment safety. Inertial cavitation is capable of causing cellular damage to endothelial cells (Miller 2007; Chen et al. 2010) and also lysis of red blood cells (Williams et al. 1991; Everbach et al. 1997).

Passive cavitation detectors can monitor the emissions generated by cavitation agents (Roy et al. 2005).

These emissions allow for ultrasound-based monitoring of cavitation therapies, and the intensity of the emissions has been found to correlate with the levels of cellular damage generated (Chen et al. 2003; Hwang et al. 2006) and blood–brain barrier opening (Tung et al. 2010; Tsai et al. 2016) where it has proved useful for feedback control (Arvanitis et al. 2012; O'Reilly and Hynynen 2012; Sun et al. 2017; Kamimura et al. 2018). However, this monitoring is limited to the confocal region between the single-element passive cavitation detector and the therapeutic ultrasound field and is therefore incapable of monitoring several locations simultaneously.

To avoid these problems, arrays of transducers can be used in combination with beamforming algorithms such as passive acoustic mapping (PAM), which uses the relative time of arrival between different elements of the array to allow for the localisation and spatial segregation between the sources of acoustic emissions in both the time (Gyöngy et al. 2008; Salgaonkar et al. 2009; Gyöngy

Address correspondence to: Constantin C. Coussios, Institute of Biomedical Engineering, University of Oxford, Old Road Campus Research Building, Oxford OX3 7 DQ, UK. E-mail: constantin.coussios@eng.ox.ac.uk

and Coussios 2010a, 2010b; O'Reilly et al. 2014) and frequency (Haworth et al. 2017; Abadi et al. 2018) domains. More recently, the development of optimized passive beamforming algorithms (Coviello et al. 2015; Lyka et al. 2016) has led to significant improvements in the spatial resolution of PAM in localizing the position and extent of cavitation both *in vitro* and *in vivo* (Choi et al. 2014; Crake et al. 2016; Paverd et al. 2019).

Since its initial development just over a decade ago, PAM has been used extensively as a qualitative tool to provide surrogate mapping of bio-effects associated with cavitation that cannot be readily monitored by ultrasound. PAM of sources of broadband or harmonic emissions was initially reported to enable both initial localization of the high-intensity focussed ultrasound focus and mapping of the location and extent of tissue ablation by cavitation-enhanced heating (Jensen et al. 2012). In the context of drug delivery, PAM of sources of broadband emissions was found to correlate well with regions of successful cavitation-mediated drug release from liposomes (Choi et al. 2014) and with regions of successful extravasation of unencapsulated therapeutics in tumours by cavitation microstreaming (Kwan et al. 2015b). In the context of reversible cavitation-mediated blood–brain barrier opening, PAM of sources of subharmonic and ultraharmonic emissions was found to correlate spatially with regions of successful extravasation on contrast magnetic resonance imaging or positron emission tomography computed tomography imaging (Arvanitis et al. 2013; Jones and Hynynen 2018; Patel et al. 2018; Yang et al. 2019). Lately, passive cavitation imaging has also been proposed as a qualitative tool for identifying regions of liquefaction after histotripsy (Bader et al. 2018) in a tissue phantom. Collectively, these contributions support the concept of cavitation dose painting to confirm both the safety and efficacy of cavitation-mediated therapies over an extended tissue region. However, these efforts are presently hindered by the absence of a setup-independent definition of a PAM-derived cavitation dose that can be directly correlated to readily measurable bio-effects.

PAM has recently been reported to be capable of producing quantitative estimates of the cavitation energy generated by sources of acoustic emissions, which can be significantly improved by accounting for diffraction effects (Gray et al. 2018), attenuation (Gray and Coussios 2018) and array-lens effects (Gray and Coussios 2019). The relationship between this PAM-derived cavitation energy and cellular safety has not previously been investigated. In this work, the spatiotemporally varying levels of cavitation generated during exposure of red blood cells to cavitation is quantified as a PAM-derived cavitation dose and related to the levels of haemolysis generated. This is achieved first in a single sample model, exploring the effect of varying the exposure and cavitation nucleation

conditions on the relationship. The experiment is then conducted using a tissue phantom containing two blood samples, investigating the ability of PAM to monitor the levels of haemolysis generated in two locations simultaneously.

METHODS

A summary of the experimental setup is provided in Figure 1. Horse blood of physiologic haematocrit (Horse Blood in acid citrate dextrose [ACD]; TCS Biosciences, Buckingham, UK) was used, which contained ACD to prevent clotting, was stored in a 4°C fridge and was used within 2 wk of harvesting. Eppendorf tubes (Eppendorf LoBind microcentrifuge tubes, volume = 2 mL; Sigma-Aldrich, Hamburg, Germany) containing samples of 0.5 mL of horse blood were mixed with one of two different types of cavitation agent at room temperature. SonoVue (SV) (Bracco, Milan, Italy) was chosen owing to its widespread use as a diagnostic contrast agent and increasingly common use across a range of therapeutic ultrasound applications (Stride and Coussios 2019).

The other agents were chosen to be gas-stabilizing, cup-shaped sub-micron solid particles, as they cavitate purely inertially and can support sustained cavitation activity for tens of minutes (Kwan et al. 2015a, 2015b), thereby providing a very different type of cavitation nucleation agent. The SonoTran particles (SPs) (OxSonics Therapeutics, Oxford, UK) were manufactured using a seed polymerization technique, producing a cup-shaped population of mean diameter 465.3 nm, poly-dispersity index 0.048 and zeta potential −37.8 mV as determined by dynamic light scattering (Zetasizer Nano ZS, Malvern Panalytical, Malvern, UK). The mean cavity size on the cups was 213 ± 15 nm as determined by transmission electron microscopy, a dimension that determines the size of the air bubbles trapped on each cup after drying and re-suspension.

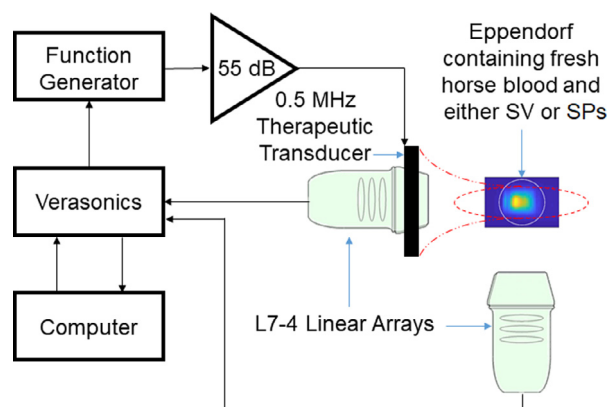


Fig. 1. Eppendorf tubes containing 0.5 mL of horse blood mixed with either SonoVue (SV) or sub-micron cavitation agent SonoTran Particles (SPs) are exposed to ultrasound for 30 s with a 5% duty cycle.

These Eppendorf tubes were placed at the focus of a 0.5-MHz therapeutic transducer (H-107 D SN12; Sonic Concepts, Bothell, WA, USA) with active diameter 64 mm and focal length 62.6 mm, and placed in a large water tank of degassed, filtered water. Two perpendicular and co-planar L7-4 linear arrays (L7-4, Verasonics, Kirkland, WA, USA) were used to simultaneously and passively capture acoustic emissions from cavitation to achieve an experimentally derived PAM resolution of 0.4 mm in both the lateral and axial directions. For this reason, 0.4 mm was chosen as the pixel size for PAM processing. To enable conversion of received electrical energy into acoustic energy, the linear arrays were calibrated with a substitution calibration using wire scattering (Gray and Coussios 2018). Data from the arrays were collected using a Verasonics Vantage Research Ultrasound System (Vantage 256, Verasonics). The samples were then exposed to peak rarefactional pressures in the range 0–2 MPa, using pulse durations in the range 50–50,000 cycles with 5% duty cycle, which have been previously shown to be effective for drug delivery across a broad range of applications from antibody (Kwan et al. 2015b) and virus (Myers et al. 2016) delivery to solid tumours, to transdermal drug and vaccine delivery (Bhatnagar et al. 2016), to blood–brain barrier opening (Kamimura et al. 2018).

Because of the different combinations of cavitation nucleation agent, exposure parameters and location within the therapeutic ultrasound field, different levels of cavitation were generated within each Eppendorf tube, which were spatiotemporally monitored using frequency domain robust capon beamforming PAM in the range 3–7 MHz. The cavitation dose observed within each sample over the duration of the exposure was then compared with the level of haemolysis. The cavitation dose was calculated as the integral of the PAM power map over the exposure duration and the measured volume within the Eppendorf tube, comprising the area of the cross section of the Eppendorf tube and the elevational full width at half-maximum of the linear arrays. This was then normalised by total treated volume (in this case the total blood volume) to give an estimate of the average cavitation energy experienced by the entire blood volume.

Two 80- μ L aliquots of each blood sample were added to 1.12 mL of phosphate-buffered saline (DPBS, Gibco, Thermofisher, MA, USA). One of the diluted aliquots was mixed with 120 μ L of 1% Triton X-100 (Triton X-100, Sigma-Aldrich) in PBS and used as a 100% reference, while the other was diluted further with 120 μ L of PBS. All samples were centrifuged at 500g at 4°C for 5 min. The absorbance of the supernatants was measured in triplicate (120 μ L per well) in a plate reader (Omega POLARStar, BMG Labtech, Ortenberg, Germany) from

220 to 1000 nm. The processing of this data can be broken down into three stages:

1. The average absorbance of three 120- μ L wells of PBS was subtracted from all the spectra to remove the effect of the PBS from the blood samples.
2. For each spectrum, the average absorbance from 750–920 nm was subtracted from the total spectra to reduce the effects of scratches on the wells; this was done as no components within the blood absorb light at these wavelengths.
3. The percentage haemolysis for each blood sample was then calculated as the absorbance at 541 nm divided by the absorbance at 541 nm for that blood sample's positive control, thereby creating an estimate of the percentage haemolysis of that sample.

An experiment was then devised to test the concept of relating spatiotemporal variations in cavitation activity in two locations being mapped simultaneously to the local bio-effects. As such a tissue phantom was designed that would allow for two blood samples to be exposed to therapeutic ultrasound pulses during simultaneous PAM mapping, thereby testing if PAM can monitor the cavitation-driven haemolysis in multiple locations simultaneously. The model (Fig. 2a) consisted of a 50 \times 50 \times 40-mm cuboid of 3% agar gel with two 4.8-mm-diameter, 30-mm-long cylindrical wells placed 8 mm apart. The Perspex cube had four acoustic windows made from Mylar sheets, thereby allowing ultrasound to pass freely both in and out. This ultrasound was generated using two identical therapeutic transducers (Fig. 2b). Each well was filled with 0.5 mL of horse blood mixed with SPs at a concentration of 1×10^{10} particles/mL.

RESULTS

Figure 3 illustrates the levels of haemolysis achieved during three parameter sweeps, a pressure sweep, a pulse length sweep (maintaining a 5 % duty cycle) and a concentration sweep with the two different cavitation agents. As was expected, increasing the pressure and concentration increased the levels of haemolysis. The peak rarefactional pressures listed are *in situ* pressures measured by direct hydrophone measurements inside the Eppendorf tube (HNA 400, Onda Corp., Sunnyvale, CA, USA). These measurements closely correspond to the free-field pressures caused by the absence of attenuating structures at 0.5 MHz in the majority of the acoustic propagation path from the transducer to the 1-cm sample contained within the thin-walled tube.

For each blood sample, PAM videos were generated so that the cavitation dose could be estimated (Fig. 4a). As expected, the cavitation energy was contained within

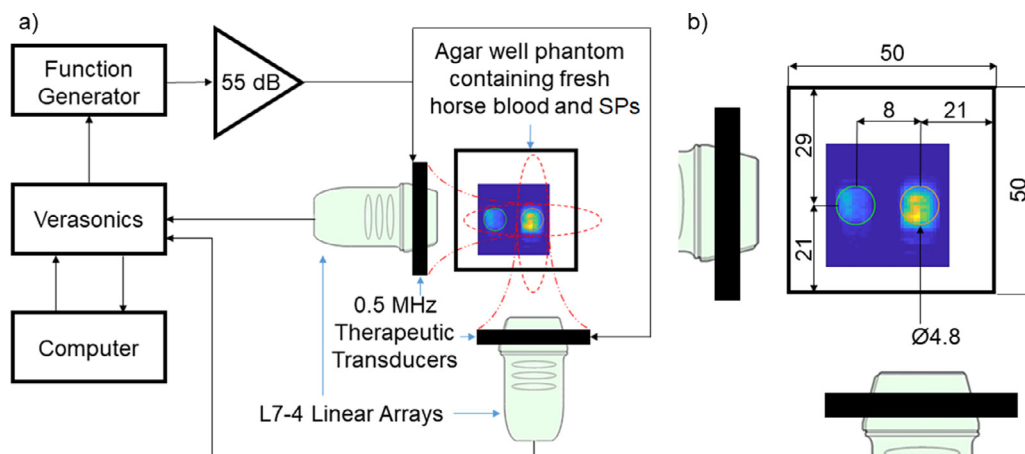


Fig. 2. Agar phantom experimental setup. (a) The agar phantom was placed with one well in the focus of two perpendicularly co-aligned 0.5-MHz therapeutic transducers, with the other well placed proximally within the full width at half-maximum of one of the transducers. (b) The phantom mould design consisted of a $50 \times 50 \times 40$ -mm cube of 3% agar gel with two 4.8-mm-diameter, 30-mm-long cylindrical wells placed 8 mm apart. All dimensions are in millimeters. SPs = SonoTran Particles.

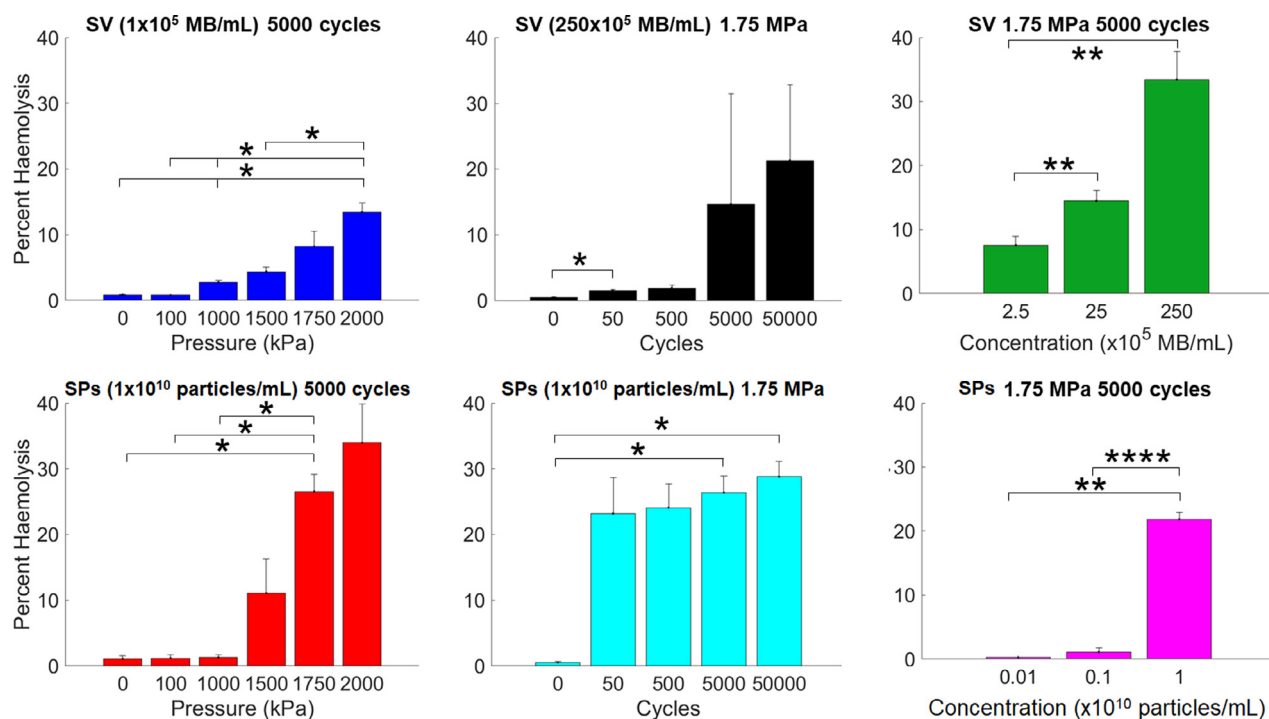


Fig. 3. Blood mixed with one of two different cavitation agents of varying concentrations and exposed to a range of ultrasound conditions for 30 s, maintaining a 5% duty cycle ($n = 3$). Error bars represent one standard deviation. Pairwise comparisons were conducted using Welch's t -test, and the p values were corrected for multiple comparisons using Hommel's method. $*p < 0.05$, $**p < 0.01$, $***p < 0.0001$. SPs = SonoTran Particles; SV = SonoVue.

the Eppendorf tube and the focal region. The SPs had sustained cavitation for the duration of the ultrasound exposure, whereas at the higher pressures, most of the SV bubbles were destroyed within the first 5 s (Fig. 4b).

To find the cavitation dose from the PAM maps, the PAM-derived power was integrated over the time of the

treatment and the 3-D measured volume, consisting of the 2-D PAM map and the elevational measurement depth of the array, and normalised by the blood volume. This made the cavitation dose measurements independent of pixel size. The relationship between the parameter sweeps and the cavitation dose can be found to be

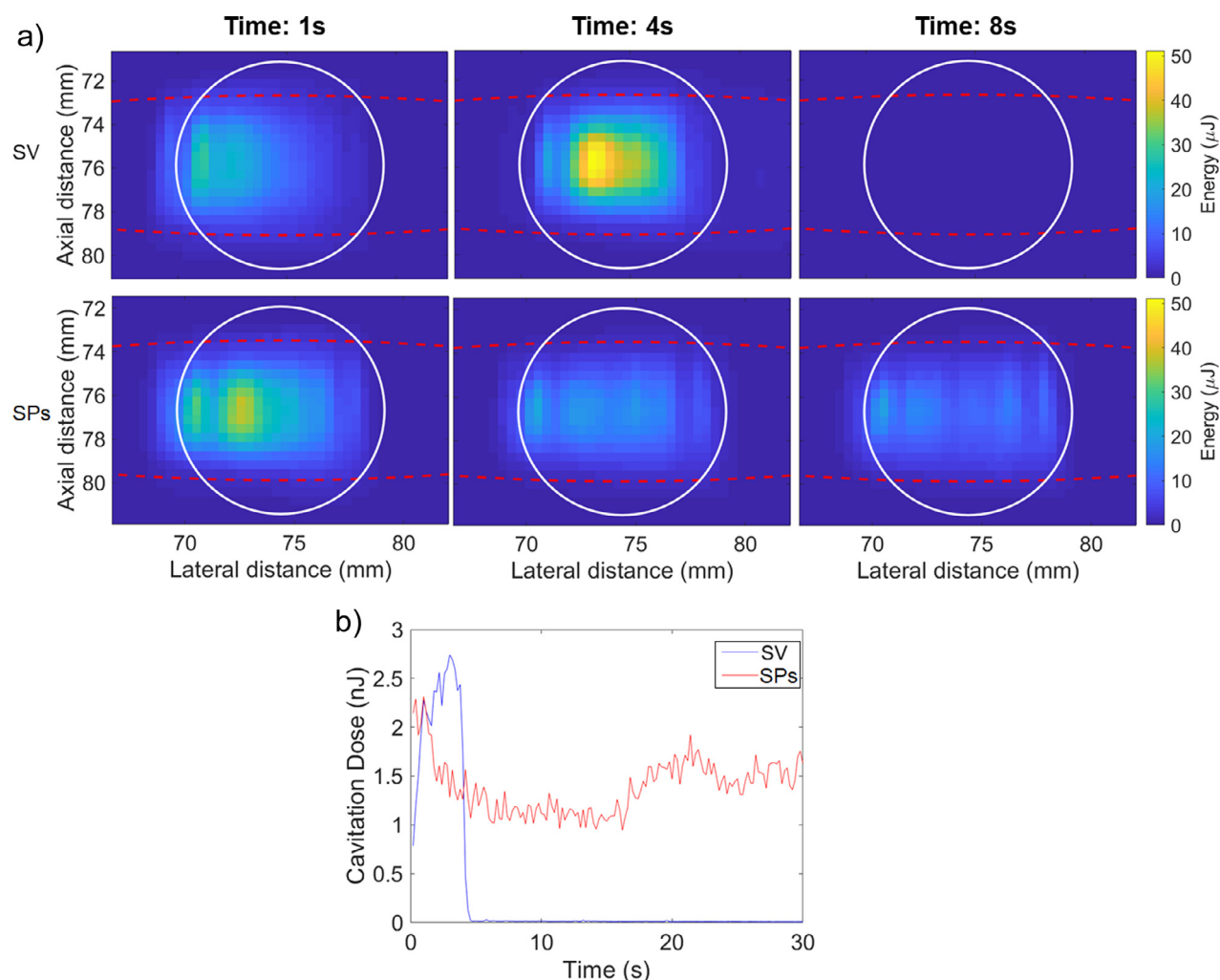


Fig. 4. (a) Frames from the passive acoustic mapping videos of the treatments. The location of the Eppendorf tube wall was estimated by B-mode, and is marked by a *white circle*. The location of the full width at half-maximum of the focal pressure was estimated using B-mode of a hydrophone tip placed in the centre of the focus, and is marked by a *red dashed oval*. Top: SonoVue (SV, 1×10^5 microbubbles [MBs]/mL) mixed with blood. Bottom: SonoTran Particles (SPs, 1×10^{10} particles/mL) mixed with blood. Obtained with 2 MPa, 5000 cycles. (b) Example cavitation dose over time for SV (1×10^5 MBs/mL) and SPs (1×10^{10} particles/mL) mixed with blood. Obtained with 2 MPa, 5000 cycles.

comparable with the relationship between the parameter sweeps and the levels of haemolysis generated (Fig. 5a). The levels of haemolysis generated in each sample can then be plotted against the cavitation dose delivered to each sample (Fig. 5b).

Blood within the tissue phantom similarly indicated that an increase in the incident pressure led to an increase in the levels of haemolysis, and as expected, the well in the middle of the focus (focal well) experienced higher levels of haemolysis than the non-focal well (Fig. 6a). Cavitation energy was contained within the wells and the focal region (Fig. 6b).

Once the cavitation dose for each blood sample was calculated, a relationship was found for every parameter sweep exhibiting an increase in haemolysis with increasing

cavitation dose. When these plots are superimposed on each other, it was found that a monotonic relationship existed that was comparable regardless of the applied pressure, pulse length, cavitation agent type or concentration used (Fig. 7).

DISCUSSION

The results of this study have a range of implications. Firstly, the fact that the extent of cavitation activity localized by PAM with a spatial resolution of $400 \mu\text{m}$ was confined to within the focal region and to within the boundaries of the Eppendorf tube that enclosed the cavitation nuclei confirms that PAM achieves high spatial specificity as a cavitation mapping tool.

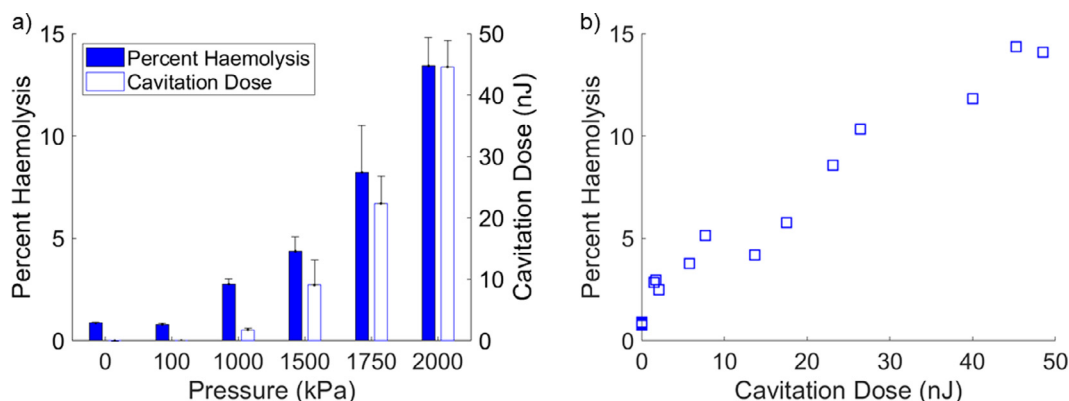


Fig. 5. Blood mixed with SonoVue (SV, 1×10^5 MBs/mL) exposed to a variety of pressures (5000 cycles, 5% duty cycle). (a) Amount of haemolysis achieved at each pressure level plotted with the total passive acoustic mapping-derived cavitation dose delivered upon exposure to each pressure level ($n = 3$). (b) Each blood sample can be plotted to find the relationship between the cavitation dose delivered and the level of haemolysis reached. Error bars represent one standard deviation.

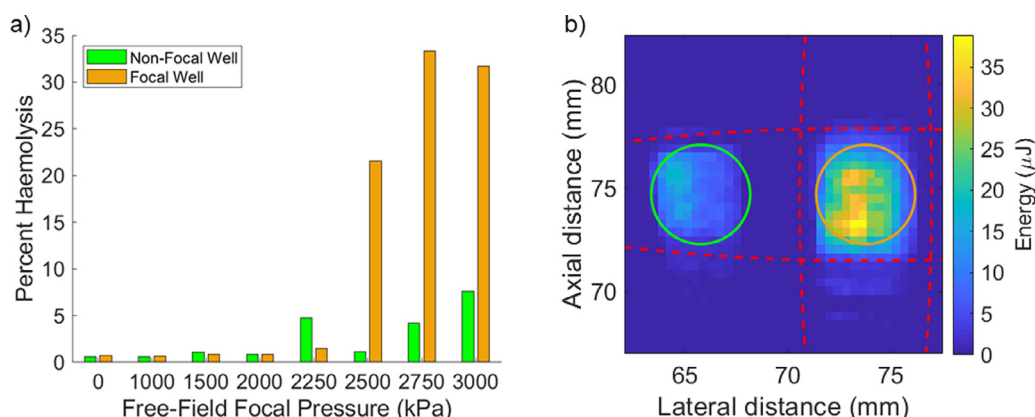


Fig. 6. Agar phantom results. (a) Levels of haemolysis achieved at each pressure level in each well. (b) Passive acoustic mapping frame from a treatment. The focal and non-focal well locations are estimated by B-mode and marked by orange and green circles, respectively. The locations of the full width at half-maximum of the focal pressures for the two transducers are marked by red dashes. Obtained with (a) SonoTran Particles (1×10^{10} particles/mL) mixed with blood and (b) 3-MPa free-field focal pressure at 5000 cycles.

PAM also allows for the tracking of the evolution of cavitation over time. Within the Eppendorf tube, the PAM videos generated when SV microbubbles were used revealed an initial increase in cavitation energy over time which then sharply dropped. One hypothesis as to why this could be the case is that initially the incident pressure field is shielded by bubbles closest to the transducer's surface. Once these bubbles are destroyed, the incident focus becomes fully formed, able to generate higher pressures in the middle of the Eppendorf tube, accelerating the destruction of microbubbles in that central region. In the case of the SPs, after the destruction of the few air bubbles within the solution, cavitation stabilises, and exclusively inertial cavitation activity is maintained throughout the treatment (Fig. 4b). These results match previous findings from the literature (Kwan et al. 2015a).

The relationship between cavitation dose and haemolysis found in this study appears linear at first (Fig. 7), eventually plateauing in the range 30%–40% haemolysis. Complete 100% haemolysis is never achieved for a number of possible reasons. Firstly, given that the focal region of the therapeutic ultrasound overlaps only with a subset of the Eppendorf tube volume, with the -6 -dB ellipsoid of the focus covering approximately 40% of the blood volume, not all red blood cells are exposed to cavitation simultaneously and there is continuous mixing caused by microstreaming between acoustically exposed regions and quiescent regions. The second factor relates to the fact that, as red blood cells are gradually lysed, the mean distance between collapsing bubbles and adjacent red blood cells increases, making the destructive interaction between inertial cavitation

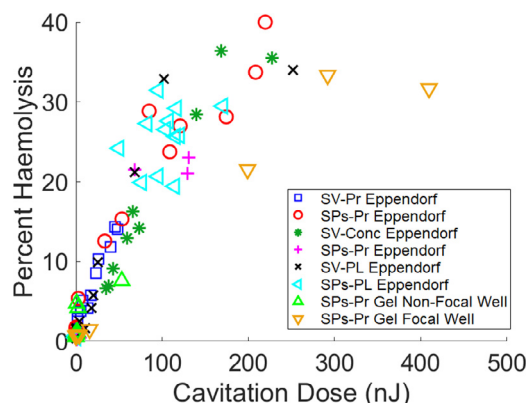


Fig. 7. A relationship was found between cavitation and haemolysis that was comparable regardless of the model (Eppendorf tube or two-well gel model) cavitation agent type (SonoVue [SV], SonoTran Particles [SPs]), concentration (Conc), applied ultrasound pressure (Pr) or pulse length (PL) used.

and lipid membranes increasingly unlikely. Other effects could also be at play, including gradual microstreaming-mediated transport of both red blood cells and cavitation nuclei out of the sample sub-volume that overlaps with the ultrasound focus. This is expected to result in a saturation and potential reduction of the haemolysis rate with increasing cavitation dose.

It is worth noting that the cavitation dose is integrated over the measured volume and normalised by the total blood volume. In the case of the models studied here, most of the total blood volume lies within the measured volume; that is, most of the total blood volume is exposed to significant levels of ultrasound. This means that the cavitation dose and levels of haemolysis experienced by the blood are up to 40%. However, if this experiment had been done *in vivo*, the ratio between the measured volume and the total blood volume would be significantly lower, as only a small sub-volume of the animal's blood is subjected to cavitation with every ultrasonic pulse. As such in an *in vivo* model, it would be expected that the average cavitation dose experienced by the blood (and, thus, the levels of haemolysis) would be significantly lower than those obtained in the experiments described here.

In the present experiment, red blood cells within the sample holder would have received 1.5 s (30 s at a 5% duty cycle) of continuous ultrasound equivalent at a focal pressure in excess of 1 MPa, and 40% of the total sample volume is exposed to cavitation on any one ultrasound pulse. *In vivo*, where flow velocities are on the order of centimeters per second, no single red blood cell is likely to be exposed to cavitation on two consecutive ultrasound pulses, and less than 5% of the total murine blood volume of 1.5 mL lies within the focal volume on any pulse. For this reason, experiments seeking to measure cavitation-mediated

haemolysis over the parameter range used in the present work *in vivo* have not yielded measurable values of free haemoglobin above background.

It is worth emphasizing that haemolysis in the context of the present work is caused intentionally to provide a metric of cellular safety, and the absolute values of haemolysis reported in the presence of microbubbles or other cavitation nuclei should therefore in no way be taken as indicative of the likely haemolysis values when using these agents *in vivo*.

The key finding of the present study was that the relationship between cavitation dose and haemolysis appears to be independent of the method by which the cavitation dose is generated, whether varying the applied pressure, pulse length, cavitation nucleation agent type or concentration. Unfortunately, it was not possible to reliably investigate the effect of varying the incident frequency over the course of the present study, because changing the frequency would also have changed the focal region size, thereby changing the fractional blood volume being haemolysed. A different experimental setup would thus be required to accurately investigate the effects of changing the incident frequency alone.

Within the limitations of the present study, the proposed metric of the total energy of acoustic emissions (in Joules) integrated over the sensing volume nevertheless appears to have considerable predictive value and makes a strong case for the need to acoustically calibrate PAM arrays on receive and adequately compensate for losses in the acoustic propagation path. This implies mechanistically that cavitation energy, as quantified by the energy of acoustic emissions, is what determines the level of haemolysis, regardless of how that energy is generated. The independence of the cavitation dose–haemolysis relationship on pressure, pulse length and local nucleation environment suggests that PAM could be used as a reliable safety monitoring tool in situations when some or all these parameters are unknown.

CONCLUSIONS

This study illustrates that PAM-derived cavitation dose, defined as the energy of acoustic emissions integrated over the measured volume, strongly correlates with cellular safety. The relationship between spatiotemporal PAM-derived cavitation dose and haemolysis depended solely on the levels of cavitation energy generated, irrespective of the pressures, pulse lengths, cavitation nucleation agent type or concentration used to achieve a particular cavitation dose level. This potentially allows for a dramatic reduction in the parameter space that needs to be considered when relating cavitation to cellular safety. These results lay the groundwork for PAM-derived cavitation-dose metrics to be applied to other measures of safety, allowing for improved ultrasound monitoring of cavitation-based therapies.

Acknowledgments—The authors thank Dr. L. Bau and Dr. M. Gray for their helpful discussions, and Jim Fisk and Dave Salisbury for their help in fabrication of the phantom mould. The authors gratefully acknowledge support from the Oxford Centre for Drug Delivery Devices (OxCD3) and a programme grant (EP/L024012/1) from the United Kingdom's Engineering and Physical Sciences Research Council, and thank OxSonics Therapeutics Ltd for provision of the SonoTran Particles used in this research.

Conflict of interest disclosure—Professor Constantin Coussios is a Founder, Director, Shareholder and receives consultancy income from OxSonics Therapeutics Ltd, a company spun out from the University of Oxford commercializing cavitation-enhanced drug delivery monitored by Passive Acoustic Mapping. Professor Coussios is also the lead inventor of granted patents on Passive Acoustic Mapping (US9238152B2 and EP2349483B8) which have been commercially licensed.

REFERENCES

- Abadi SH, Haworth KJ, Mercado-Shekhar KP, Dowling DR. Frequency-sum beamforming for passive cavitation imaging. *J Acoust Soc Am* 2018;144:198–209.
- Arvanitis CD, Livingstone MS, Vykhotseva N, McDannold N. Controlled ultrasound-induced blood–brain barrier disruption using passive acoustic emissions monitoring. *PLoS One* 2012;7:e45783.
- Arvanitis CD, Livingstone MS, McDannold N. Combined ultrasound and MR imaging to guide focused ultrasound therapies in the brain. *Phys Med Biol* 2013;58:4749–4761.
- Bader KB, Haworth KJ, Maxwell AD, Holland CK. Post hoc analysis of passive cavitation imaging for classification of histotripsy-induced liquefaction in vitro. *IEEE Trans Med Imaging* 2018;37:106–115.
- Bazan-Peregrino M, Rifai B, Carlisle RC, Choi J, Arvanitis CD, Seymour LW, Coussios CC. Cavitation-enhanced delivery of a replicating oncolytic adenovirus to tumors using focused ultrasound. *J Control Release* 2013;169:40–47.
- Bhatnagar S, Kwan JJ, Shah AR, Coussios CC, Carlisle RC. Exploitation of sub-micron cavitation nuclei to enhance ultrasound-mediated transdermal transport and penetration of vaccines. *J Control Release* 2016;238:22–30.
- Bian S, Seth A, Daly D, Carlisle R, Stride E. A multimodal instrument for real-time in situ study of ultrasound and cavitation mediated drug delivery. *Rev Sci Instrum* 2017;88(3):34302.
- Chen WS, Brayman AA, Matula TJ, Crum LA. Inertial cavitation dose and hemolysis produced in vitro with or without Optison. *Ultrasound Med Biol* 2003;29:725–737.
- Chen H, Brayman AA, Bailey MR, Matula TJ. Blood vessel rupture by cavitation. *Urol Res* 2010;38:321–326.
- Choi JJ, Carlisle RC, Coviello C, Seymour L, Coussios CC. Non-invasive and real-time passive acoustic mapping of ultrasound-mediated drug delivery. *Phys Med Biol* 2014;59:4861–4877.
- Coviello C, Kozick R, Choi J, Gyöngy M, Jensen C, Smith PP, Coussios CC. Passive acoustic mapping utilizing optimal beamforming in ultrasound therapy monitoring. *J Acoust Soc Am* 2015;137:2573.
- Crake C, Owen J, Smart S, Coviello C, Coussios CC, Carlisle R, Stride E. Enhancement and passive acoustic mapping of cavitation from fluorescently tagged magnetic resonance-visible magnetic microbubbles in vivo. *Ultrasound Med Biol* 2016;42:3022–3036.
- Everbach EC, Makin IRS, Azadniv M, Meltzer RS. Correlation of ultrasound-induced hemolysis with cavitation detector output in vitro. *Ultrasound Med Biol* 1997;23:619–624.
- Fan Z, Liu H, Mayer M, Deng CCX. Spatiotemporally controlled single cell sonoporation. *Proc Natl Acad Sci USA* 2012;109:16486–16491.
- Gray MD, Coussios CC. Broadband ultrasonic attenuation estimation and compensation with passive acoustic mapping. *IEEE Trans Ultrason Ferroelectr Freq Control* 2018;65:1997–2011.
- Gray MD, Coussios CC. Compensation of array lens effects for improved co-registration of passive acoustic mapping and B-mode images for cavitation monitoring. *J Acoust Soc Am* 2019;146:EL78–EL84.
- Gray MD, Lyka E, Coussios CC. Diffraction effects and compensation in passive acoustic mapping. *IEEE Trans Ultrason Ferroelectr Freq Control* 2018;65:258–268.
- Gyöngy M, Coussios CC. Passive spatial mapping of inertial cavitation during HIFU exposure. *IEEE Trans Biomed Eng* 2010a;57:48–56.
- Gyöngy M, Coussios CC. Passive cavitation mapping for localization and tracking of bubble dynamics. *J Acoust Soc Am* 2010b;128:EL175–EL180.
- Gyöngy M, Arora M, Noble JA, Coussios CC. Use of passive arrays for characterization and mapping of cavitation activity during hifu exposure. *Proc IEEE Int Ultrason Symp* 2008;871–874.
- Haworth KJ, Bader KB, Rich KT, Holland CK, Mast TD. Quantitative frequency-domain passive cavitation imaging. *IEEE Trans Ultrason Ferroelectr Freq Control* 2017;64:177–191.
- Hwang JH, Tu J, Brayman AA, Matula TJ, Crum LA. Correlation between inertial cavitation dose and endothelial cell damage in vivo. *Ultrasound Med Biol* 2006;32:1611–1619.
- Hynynen K, McDannold N, Vykhotseva N, Jolesz FA. Noninvasive MR imaging—guided focal opening of the blood–brain barrier in rabbits. *Radiology* 2001;220:640–646.
- Jensen CR, Ritchie RW, Gyöngy M, Collin JRT, Leslie T, Coussios CC. Spatiotemporal monitoring of high-intensity focused ultrasound therapy with passive acoustic mapping. *Radiology* 2012;262:252–261.
- Jones RM, Hynynen K. Advances in acoustic monitoring and control of focused ultrasound-mediated increases in blood–brain barrier permeability. *Br J Radiol* 2018;92:20180601.
- Kamimura HAS, Flament J, Valette J, Cafarelli A, Aron Badin R, Hantraye P, Larrat B. Feedback control of microbubble cavitation for ultrasound-mediated blood–brain barrier disruption in non-human primates under magnetic resonance guidance. *J Cereb Blood Flow Metab* 2018;39:1191–1203.
- Kwan JJ, Graham S, Myers R, Carlisle R, Stride E, Coussios CC. Ultrasound-induced inertial cavitation from gas-stabilizing nanoparticles. *Phys Rev E* 2015a;92:23019.
- Kwan JJ, Myers R, Coviello CM, Graham SM, Shah AR, Stride E, Carlisle RC, Coussios CC. Ultrasound-propelled nanocups for drug delivery. *Small* 2015b;11:5305–5314.
- Lyka E, Coviello C, Kozick R, Coussios CC. Sum-of-harmonics method for improved narrowband and broadband signal quantification during passive monitoring of ultrasound therapies. *J Acoust Soc Am* 2016;140:741–754.
- Mannaris C, Teo BM, Seth A, Bau L, Coussios C, Stride E. Gas-stabilizing gold nanocones for acoustically mediated drug delivery. *Adv Healthc Mater* 2018;7:e1800184.
- Miller DL. Overview of experimental studies of biological effects of medical ultrasound caused by gas body activation and inertial cavitation. *Prog Biophys Mol Biol* 2007;93:314–330.
- Myers R, Coviello C, Erbs P, Foloppe J, Rowe C, Kwan J, Crake C, Finn S, Jackson E, Balloul JM, Story C, Coussios C, Carlisle R. Polymeric cups for cavitation-mediated delivery of oncolytic vaccinia virus. *Mol Ther* 2016;24:1627–1633.
- O'Reilly MA, Hynynen K. Blood–brain barrier: Real-time feedback-controlled focused ultrasound disruption by using an acoustic emissions–based controller. *Radiology* 2012;263:96–106.
- O'Reilly MA, Jones RM, Hynynen K. Three-dimensional transcranial ultrasound imaging of microbubble clouds using a sparse hemispherical array. *IEEE Trans Biomed Eng* 2014;61:1285–1294.
- Patel A, Schoen SJ, Jr, Arvanitis CD. Closed loop spatial and temporal control of cavitation activity with passive acoustic mapping. *IEEE Trans Biomed Eng* 2018;66:2022–2031.
- Pavard C, Lyka E, Elbes D, Coussios C. Passive acoustic mapping of extravasation following ultrasound-enhanced drug delivery. *Phys Med Biol* 2019;64:045006.
- Roy RA, Madanshetty SI, Apfel RE. An acoustic backscattering technique for the detection of transient cavitation produced by microsecond pulses of ultrasound. *J Acoust Soc Am* 2005;87:2451–2458.

- Salgaonkar VA, Datta S, Holland CK, Mast TD. Passive cavitation imaging with ultrasound arrays. *J Acoust Soc Am* 2009;126:3071–3083.
- Stride E, Coussios C. Nucleation, mapping and control of cavitation for drug delivery. *Nat Rev Phys* 2019;1:495–509.
- Sun T, Zhang Y, Power C, Alexander PM, Sutton JT, Aryal M. Closed-loop control of targeted ultrasound drug delivery across the blood–brain/tumor barriers in a rat glioma model. *Proc Natl Acad Sci USA* 2017;114:E10281–E10290.
- Sutton JT, Haworth KJ, Pyne-Geithman G, Holland CK. Ultrasound-mediated drug delivery for cardiovascular disease. *Expert Opin Drug Deliv* 2013;10:573–592.
- Tsai CH, Zhang JW, Liao YY, Liu HL. Real-time monitoring of focused ultrasound blood–brain barrier opening via subharmonic acoustic emission detection: Implementation of confocal dual-frequency piezoelectric transducers. *Phys Med Biol* 2016;61:2926–2946.
- Tung YS, Vlachos F, Choi JJ, Deffieux T, Selert K, Konofagou EE. In vivo transcranial cavitation threshold detection during ultrasound-induced blood–brain barrier opening in mice. *Phys Med Biol* 2010;55:6141–6155.
- Williams AR, Kubowicz G, Cramer E, Schleif R. The effects of the microbubble suspension SH U 454 (Echovist) on ultrasound-induced cell lysis in a rotating tube exposure system. *Echocardiography* 1991;8:423–433.
- Yang Y, Zhang X, Ye D, Laforest R, Williamson J, Liu Y, Chen H. Cavitation dose painting for focused ultrasound-induced blood–brain barrier disruption. *Sci Rep* 2019;9:2840.